

magnetic field enhancements associated with surface plasmon resonances over the non-enhanced Raman scattering methods. However, SERS requires the target molecule to adsorb onto a metal surface to benefit from surface plasmon resonance. Consequently, it has been difficult to detect biological molecules that have a low affinity for metal surfaces, and only a few types of molecules have been detected by SERS with single-molecule sensitivity to date. The researchers said that huge signal gain can be obtained by combining SERS and coherent anti-Stokes Raman scattering (CARS) as is done in surface-enhanced coherent anti-Stokes Raman scattering (SECARS). The researchers further improved the sensitivity of SECARS over the earlier reported work, and achieved single-molecule detection of some biomolecules not detected earlier using this method.

The researchers said that SECARS background originating from metal and water has limited the sensitivity of previous works. The research group used several methods, such as a polarization-sensitive CARS setup, minimized probe volume, and the use of aggregated colloidal silver nanoparticles instead of planar substrates, to reduce the background. The SECARS signals of biological molecules were increased by the addition of lithium chloride salts, which were found to be optimal for generating strong surface enhancements.

The researchers then demonstrated the power of SECARS by detecting two DNA nucleotides, deoxyadenosine monophosphate (dAMP) and deoxyguanosine monophosphate (dGMP), and a peptide—angiotensin-I peptide. Although dAMP has been detected at the single-molecule level by SERS, the SECARS signal was approximately 1000 times stronger than the SERS signal for dAMP at single-molecule concentrations. The SECARS signal of dGMP was at least 100 times stronger than the SERS signal of dGMP. The researchers believe that this is the first reported detection of dGMP at single-molecule concentrations.

The detection of the peptide shows that the SECARS technique can be applied to biological molecules other than nucleotides. According to the research group, the ultrasensitive detection of nonlabeled peptides and proteins has potential applications in pathogen detection, disease monitoring, and drug discovery.

VIVEK RANJAN

### Cell Membranes Integrated into CNT Devices

Integrating biological systems and

processes with nanofabricated structures is a critical challenge for nanotechnology. In the May issue of *Nano Letters*, J.-C. Gabriel, G. Grüner, and their co-workers reported on their work, performed at Nanomix Inc., on the integration of the cell membrane of *Halobacterium salinarum* with carbon nanotube (CNT) network transistors, wherein both the biological and nanoelectronic structures preserve their functionality and are able to electronically interact with each other.

The researchers fabricated nanotube network field-effect transistors, where the semiconducting channel is formed by a network of predominantly semiconducting nanotubes. A monolayer of the purple membrane from *Halobacterium salinarum* was then deposited on the exposed semiconductor channel. Evidence for the integration of the membrane with the device comes from changes in the device characteristics of the transistor.

The purple membrane contains bacteriorhodopsin, which has a permanent electric dipole moment pointing from the extracellular side of the membrane toward the cytoplasmic side. The researchers prepared three sets of devices. The first had the membrane dipole randomly oriented on the nanotubes, while the second and third sets had the cytoplasmic or extracellular side of the membrane facing the nanotubes. Prior to integration of the membrane, the nanotube devices by themselves worked as *p*-type transistors with good conduction at negative gate voltages and no conduction at positive gate voltages. The voltage at which the device turns on is known as the threshold voltage and is different depending on the sweep direction of the gate voltage (i.e., it is hysteretic). The hysteresis is known to be produced by water adsorbed on the substrate.

For the mixed-orientation nanobioelectronic device, deposition of the cell membrane resulted in a narrower hysteresis compared with the hysteresis of the nanotube devices alone. The researchers attributed this effect to desorption of water from the nanotube surface as the membrane displaced water. Also, the turn on for this device was less sharp, indicating a change in carrier mobility for the nanotube networks arising from random scattering potentials due to the electric dipoles of rhodopsin. The oriented membrane devices also showed a loss of hysteresis and a shift of the threshold voltage in different directions for the two different orientations of the membrane. Since the threshold voltage is correlated to the position of the Fermi level in nanotubes, the shift in the threshold voltage is indicative of a charge induced in the nanotube

by the electric dipole of the membrane. The magnitudes of the shifts are different for the two orientations, implying asymmetry in the charge distribution of rhodopsin, with the dipole being closer to the cytoplasmic side.

Grüner, who is a professor at UCLA and advisor to the project, said that this work “opens up avenues for what could be called ‘cellectronics,’ the electronic detection and also modification of biological processes at the cellular level.”

SARBAJIT BANERJEE

### Continuous-Wave 1.94 $\mu\text{m}$ Laser Based on Tm:BaY<sub>2</sub>F<sub>8</sub> Lasers from 1849 nm to 2059 nm

Efficient, widely tunable solid-state laser sources in the near-infrared region around 2  $\mu\text{m}$  have potential applications in remote sensing and gas detection, high-resolution spectroscopy, frequency metrology, and medicine. Thulium doping of crystals can be used in this wavelength region because of the  $^3\text{F}_4\text{--}^3\text{H}_6$  optical transition of Tm<sup>3+</sup> ions that in most host media yields a very broad emission with a maximum at wavelengths of ~1.8–1.9  $\mu\text{m}$ . In addition, Tm<sup>3+</sup> has the advantage that it can be directly diode-pumped at ~785 nm, and shows a quantum efficiency close to 2 (i.e., each pump quantum absorbed yields two Tm ions in the upper laser level).

In the April 15 issue of *Optics Letters* (p. 854), G. Galzerano and P. Laporta of Politecnico di Milano, in a joint collaboration with M. Tonelli and colleagues from the Università di Pisa, Italy, described the growth, spectroscopic characterization, and laser action of a diode-pumped laser based on a Tm-doped fluoride crystal (Tm:BaY<sub>2</sub>F<sub>8</sub>). They reported a room-temperature, diode-pumped laser oscillator widely tunable over a 210 nm interval, from 1849 nm to 2059 nm, with a maximum continuous-wave (cw) output power of ~150 mW at 1920 nm by use of a 0.5% output coupler transmission.

The researchers said that fluoride crystals, despite thermomechanical properties that are usually poorer than those of most oxides, present some advantages in terms of laser performance. These include low phonon energy, longer fluorescence lifetime, lower upconversion losses, reduced thermal lensing, and extremely low-beam depolarization under strong pumping. The crystal was grown in a homemade Czochralski furnace, starting with BaY<sub>2</sub>F<sub>8</sub> powder and adding BaF<sub>2</sub> and TmF<sub>3</sub> powders. The best laser results were obtained for a Tm doping level of 12%. Crystallinity and crystallographic orientation were determined from x-ray

Laue results, which enabled the preparation of oriented samples.

The laser resonator was a three-mirror folded cavity configuration to allow compensation of a slight astigmatism introduced by the laser crystal. The 2.2-mm-long laser crystal was placed at a Brewster's angle close to the plane high-reflectivity mirror and was mounted on a copper heat sink without any cooling system. The  $\text{Tm:BaY}_2\text{F}_8$  was longitudinally pumped by a GaAlAs laser diode at a wavelength of  $\sim 780$  nm with a maximum cw output power of 3 W. Tuning of the laser wavelength was accomplished by adjustment of an intracavity quartz plate acting as a birefringent filter. The free-running laser showed cw oscillation over a wide range of wavelengths that depended on the specific configuration. Increasing the output coupling increased the output power, but decreased the wavelength tuning range. The lower-wavelength end of the tuning range (i.e., 1850 nm) was limited by the bandwidth of the dielectric laser mirrors that were used. The wavelength-shift of up to 2059 nm, compared with the longest emission wavelength observed in the fluorescence spectrum, at 1925 nm, is ascribed to the vibronic behavior of the laser crystal. To the researchers' knowledge, this is the largest shift ever observed for a rare-earth laser.

ROSALÍA SERNA

### Nanotube Coupled with Nanodiamond Forms Hybrid Nanomaterial

The increasing scale of device integration in solid-state technology, coinciding with decreasing structure dimensions, requires the use of nanomaterials that can be engineered to form nanoscale architectures, built from units with desired shapes and properties. Moreover, such materials must survive under severe conditions. In this context, the family of carbon nanostructures is ideally suited for a wide range of innovative applications, and their chemical compatibility makes hybrid nanomaterials that couple nanotubes and nanodiamond an attractive prospect. Recently, M.L. Terranova and colleagues of the University of Rome

"Tor Vergata," M. Rossi of the University of Rome "La Sapienza," and A.S. Barnard of Argonne National Laboratory have produced ordered deposits of tubular nanostructured carbon that couple diamond nanocrystals with single-walled carbon nanotubes.

In a forthcoming issue of *Chemistry of Materials* (DOI: 10.1021/cm0502018), Terranova, Rossi, and colleagues outlined a systematic method for the growth of these hybrid nanocarbons, involving the reaction of graphitic carbon nanopowders (produced by cw-laser-assisted pyrolysis of hydrocarbon mixtures) with atomic H, in a modified chemical vapor deposition reactor. The carbon nanopowders were carried from a reservoir by Ar streams and homogeneously delivered across the active area of a Si substrate coated by a sub-micron dispersion of Fe particles. The experimental parameters were outlined, and it was shown that under well-defined conditions, the production of ordered arrays of rigid nanotubes coated by diamond nanocrystals was possible during the same run. The final deposits consisted of vertically aligned, tubular bundles of single-walled carbon nanotubes up to 15  $\mu\text{m}$  long, coated with an outer deposit of well-shaped diamond nanocrystals (see Figure 1), attached to the nanotubes by a reduced portion of their base. To facilitate the investigation of the formation of these materials, the researchers constructed a time-growth sequence by ad hoc experiments performed by changing the duration of the synthesis process in the range of 1–15 min. The samples for each deposition time were characterized, and the growth and evolution of each of the respective nanocarbon phases were confirmed.

The researchers proposed that following nanotube growth, the high relative concentration of atomic H used in the experiments was instrumental in disrupting locally the C–C  $sp^2$  network of the nanotube walls, thereby creating localized C–C  $sp^3$  defects that act as suitable sites for the nucleation of diamond nanocrystals. As soon as the first diamond crystallites were formed, further top-growth of the nanotube was repressed, since further buildup of nano-

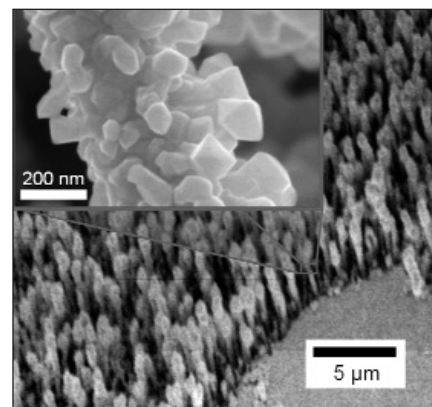



Figure 1. Vertically aligned, tubular bundles of single-walled carbon nanotubes up to 15  $\mu\text{m}$  long, coated with an outer deposit of 20–100 nm of nanodiamond, along with a detailed image (inset) showing the faceted shape of the diamond nanocrystals.

tubes was limited by the initial coverage of diamond nanocrystals. Following crystallization, the nanodiamond growth continued, taking advantage of the surface supersaturation and localized carbon segregation produced by the etching of some of the nanotubes as well as that of the feeding C nanopowders. The final coating of diamond nanocrystals remained as "hanging objects," due to the curvature of the (nanotube) substrate, with typical sizes ranging from 20 nm near the base of the nanotubes to 100 nm at the top.

Considering that diamond is one of the most promising wide-bandgap semiconductors for various electronic devices, with an excellent potential due to its negative electron affinity, the researchers said that these rigid rods may find applications as micro- and nanoscale cold-cathode devices, miniaturized cathode-ray tubes, light-emitting displays, micromechanics, and nanoscale sensing.

For more research news on Materials Science, access the Materials Research Society Web site: [www.mrs.org/connections](http://www.mrs.org/connections)



**Experience the interactive materials science exhibition:**

**Cranbrook Institute of Science, Bloomfield Hills, MI**  
June 4 – September 5, 2005

**Dallas Museum of Natural History Dallas, TX**  
May 21 – Sept. 4, 2005

To volunteer for activities with the exhibition, contact  
**Amy Moll**  
Community Resources Coordinator, [amoll@boisestate.edu](mailto:amoll@boisestate.edu)

Strange Matter is presented by the Materials Research Society. This exhibition and its tour are made possible by the generous support of the National Science Foundation, Alcan Inc., Dow, Ford Motor Company Fund, Intel Innovation In Education, and the 3M Foundation.

